



Published in final edited form as:

*Ann Biomed Eng.* 2021 December ; 49(12): 3711–3723. doi:10.1007/s10439-021-02772-5.

## Pre-surgical Prediction of Ischemic Mitral Regurgitation Recurrence Using *In Vivo* Mitral Valve Leaflet Strains

HARSHITA NARANG<sup>1</sup>, BRUNO V. REGO<sup>1</sup>, AMIR H. KHALIGHI<sup>1</sup>, AHMED ALY<sup>2</sup>, ALISON M. POUCH<sup>2</sup>, ROBERT C. GORMAN<sup>2</sup>, JOSEPH H. GORMAN III<sup>2</sup>, MICHAEL S. SACKS<sup>1</sup>

<sup>1</sup>James T. Willerson Center for Cardiovascular Modeling and Simulation, Oden Institute for Computational Engineering and Sciences, Department of Biomedical Engineering, The University of Texas at Austin, Austin, TX, USA

<sup>2</sup>Gorman Cardiovascular Research Group, Smilow Center for Translational Research, Department of Surgery, Perelman School of Medicine, University of Pennsylvania, Philadelphia, PA, USA

### Abstract

Ischemic mitral regurgitation (IMR) is a prevalent cardiac disease associated with substantial morbidity and mortality. Contemporary surgical treatments continue to have limited long-term success, in part due to the complex and multi-factorial nature of IMR. There is thus a need to better understand IMR etiology to guide optimal patient specific treatments. Herein, we applied our finite element-based shape-matching technique to non-invasively estimate peak systolic leaflet strains in human mitral valves (MVs) from *in-vivo* 3D echocardiographic images taken immediately prior to and post-annuloplasty repair. From a total of 21 MVs, we found statistically significant differences in pre-surgical MV size, shape, and deformation patterns between the with and without IMR recurrence patient groups at 6 months post-surgery. Recurrent MVs had significantly less compressive circumferential strains in the anterior commissure region compared to the recurrent MVs ( $p = 0.0223$ ) and were significantly larger. A logistic regression analysis revealed that average pre-surgical circumferential leaflet strain in the Carpentier A1 region independently predicted 6-month recurrence of IMR (optimal cutoff value – 18%,  $p = 0.0362$ ). Collectively, these results suggest greater disease progression in the recurrent group and underscore the highly patient-specific nature of IMR. Importantly, the ability to identify such factors pre-surgically could be used to guide optimal treatment methods to reduce post-surgical IMR recurrence.

### Keywords

Ischemic mitral regurgitation; Finite element method; Transesophageal echocardiography

---

Address correspondence to Michael S. Sacks, James T. Willerson Center for Cardiovascular Modeling and Simulation, Oden Institute for Computational Engineering and Sciences, Department of Biomedical Engineering, The University of Texas at Austin, Austin, TX, USA. msacks@oden.utexas.edu.

#### SUPPLEMENTARY INFORMATION

The online version contains supplementary material available at <https://doi.org/10.1007/s10439-021-02772-5>.

#### CONFLICT OF INTEREST

The authors declare they have no conflict of interest.

## INTRODUCTION

The mitral heart valve (MV) withstands some of the most intense loading conditions in the body.<sup>9,21,36,37</sup> and despite its phenomenal durability, approximately 2% of the US population suffers from a MV disease.<sup>29</sup> A particularly deadly form of MV disease is ischemic mitral regurgitation (IMR), which affects over 1.5 million Americans.<sup>30</sup> In contrast to primary or degenerative mitral regurgitation, IMR is intrinsically a disease of the left ventricle (LV), as it occurs secondary to a myocardial infarction (MI). The geometric changes that occur in IMR, especially leaflet tethering caused by downward displacement of the papillary muscles and annular dilation, cause critical changes to the kinematics of the MV, changing the deformations and loads experienced by the system and leading to long-term plastic deformations and remodeling.<sup>3,6,8,20,40</sup> The two primary clinical options for mitigating the effects of chronic IMR are MV repair and replacement.<sup>1,2,7,11,14,24,26</sup> While both have high rates of failure, some studies have found repairs to perform substantially worse within the first year post-surgery, reporting failure rates as high as 60%.<sup>10,15,28,40</sup> Repair has become preferred to replacement for IMR as it better preserves MV function; however, despite promising initial surgical outcomes and the use of concomitant procedures, the rate of long-term failure remains high.<sup>1,24,27</sup>

Advances in real-time clinical echocardiographic imaging have improved our ability to extract MV geometrical characteristics over the cardiac cycle. A recent study used such data to quantify the patient-specific risk of MR recurrence at 6 months post-surgery and found that preoperative MV leaflet tethering angle in the P3 Carpentier segment was significantly different between the groups of MVs with and without IMR recurrence.<sup>6</sup> This exciting result suggests that there are detectable differences in the pre-surgical functional state of regurgitant MVs in patients that respond well to undersized ring annuloplasty (URA). Importantly, it also underscores the potential of pre-surgically obtained geometric predictors of 6-month MR recurrence, suggesting that patient-specific pre-surgical assessment could be used to improve evaluation of risk during surgical planning and help guide MV repair methods for improved outcomes.<sup>1,6</sup>

Since the MV is a highly integrated and functionally complex structure, however, more advanced approaches that derive the full 3D functional characteristics of the MV are clearly needed.<sup>38</sup> This need is underscored by studies of the *in vitro* and *in vivo* deformation of the MV,<sup>35</sup> which reveal complex dynamics in health and disease. We recently developed a novel *noninvasive* method of strain estimation which uses real-time three-dimensional transesophageal echocardiographic (rt-3DE) images and an elasticity-based finite element (FE) framework for determining the complete in-plane surface strains during MV closure.<sup>33</sup> By applying this technique to the ovine MV in the normal and post-MI states,<sup>31</sup> we found that the majority of changes in systolic stretch fields and increases in MV size occur within the first four weeks after MI onset, with IMR inducing permanent changes in leaflet diastolic shape and substantially reducing peak systolic stretch. These results demonstrated that the kinematic behavior of the MV changes progressively and substantially in the post-MI period. Moreover, we have recently demonstrated in an ovine model of IMR that the MV leaflet tissue undergoes an isotropic irreversible plastic deformation, along with underlying changes

in transcriptomic responses.<sup>16,31,32</sup> Such permanent changes may also affect the success of the repair surgery, as it is unknown how the altered MV leaflet tissue responds to the altered stress states following MV repair.

The above findings motivated us to apply our noninvasive MV strain estimation method to further our understanding of the human MV post-MI in the present study. Our goal was to assess the MV pre-surgical systolic deformation state in patients who have undergone MV repair surgery in order to determine whether pre-surgical deformation patterns are predictive of post-surgical outcomes. We compared several metrics MV with and without repair failure at 6 months post-surgery. Deriving factors that play a role in predicting repair success could help elucidate underlying mechanisms of disease progression, lay the basis for more advanced models of surgical repair, and improve surgical techniques and planning on a patient-specific basis.

## METHODS

### Image Acquisition

Clinical rt-3DE images from a preexisting database were used for this study.<sup>6</sup> Images were obtained through a mid-esophageal view in 3 individuals without IMR and immediately before and after a URA repair procedure in 18 patients with IMR. Of the patients with IMR, 11 had no recurrence of MR at 6 months post-repair and 7 had recurrence at this time point. All patients had grade 3 or 4 IMR prior to surgery (moderate-severe to severe). Recurrent IMR was defined as an MR grade of 2 (moderate) or higher at 6 months post-surgery. Each image contained approximately 6–12 frames per cardiac cycle over 2–3 consecutive cycles, with an approximate voxel resolution of 0.6 to 0.8mm. Details of the image acquisition methods have been described previously.<sup>6</sup> Of the available data, only images with fully visible MV leaflets were used in this study.

### Image Segmentation and FE Mesh Generation

Images were exported in Cartesian format and representative frames at end-diastole (ED, fully open MV) and at end-systole (ES, fully closed MV) were selected for segmentation. The selected frames were segmented using an interactive program (Fig. 1). For each image, the annular plane was first rotated to a short-axis view and the geometric center of the MV orifice was translated to the intersection of two long-axis planes corresponding to the intercommissural and septolateral axes of the MV orifice. Several septolateral long-axis cross-sections were made along the intercommissural axis approximately 1 mm apart. At each cross-section, the anterior and posterior leaflet were traced separately along the midsurface of the tissue from the annulus to the free edge. Each image was segmented to include as much of the commissure region as possible, using only identifiable leaflet tissue. The methods used to develop a mesh from the segmented images have been described in detail previously.<sup>33</sup> Briefly, the points in each curve were connected using shape-preserving piecewise cubic spline interpolation. Each curve was then rediscritized into segments of equal arc length and developed into a mesh using 2D Delaunay triangulation, Poisson-disk sampling, ball-pivoting reconstruction, and Taubin smoothing algorithms. Small regional gaps at the commissures were interpolated when necessary. This resulted in meshes with

uniform, unstructured nodal distributions, nodes spaced approximately 1mm apart, and approximately 2000 elements per mesh.

### FE-Based Shape-Matching Method for Planar Strain Estimation

The individual MV leaflets are difficult to identify in the coaptation zone of the closed MV in rt-3DE images, and meshing the ED and ES states separately results in different distributions and connectivity of nodes, preventing determination of the local strain field. In order to build a direct material point correspondence of the MV leaflets between the open and closed states, we morphed the ED mesh of each MV into the corresponding ES shape through a FE simulation. Our FE-based shape-matching technique, summarized in the following, has been previously extensively validated using high fidelity microCT data,<sup>17</sup> as well as *in-vivo* strain data,<sup>36</sup> with excellent agreement in both cases.<sup>33</sup> When we applied this technique in the present study, we found negligible differences in the computed in-surface leaflet strains between different segmentations of the same valve in the same state. This was the case even where the commissural leaflet tissue was slightly shorter, longer, or had unusual geometries.

All shape-matching simulations were performed using the commercial FE software package Abaqus 6.13 (Dassault Systèmes), configured to use a Newton-Raphson nonlinear quasistatic solver with explicit central difference time integration and automatic time stepping. Frictionless self-contact of the MV leaflet surface was enforced. The triangulated leaflet mesh was defined to have isoparametric shell elements. It is important to note that in the present approach, the use of tissue elasticity only served to regularize the morphing process of the MV geometry. Thus in this approach, the shape-matching model does not require precise material properties. We used a nearly incompressible isotropic constitutive model which has been found to be sufficient to model MV tissue.<sup>12,22</sup> The second Piola-Kirchhoff stress tensor,  $\mathbf{S}$ , was defined as

$$\mathbf{S} = \frac{1}{\pi} \int_{-\pi/2}^{\pi/2} S_{\text{ens}}[E_{\text{ens}}(\theta)] \mathbf{n}(\theta) \otimes \mathbf{n}(\theta) d\theta + \mu_m (\mathbf{I} - C_{33} \mathbf{C}^{-1}) \quad (1)$$

where  $\mathbf{E} = (\mathbf{C} - \mathbf{I})/2$  is the Green-Lagrange strain tensor,  $\mathbf{n}$  is a unit vector describing the alignment of a family of collagen fibers,  $S_{\text{ens}}$  and  $E_{\text{ens}} = \mathbf{n}^T \mathbf{E} \mathbf{n}$  are the second Piola-Kirchhoff stress and Green-Lagrange strain respectively along the ensemble direction  $\hat{\mathbf{n}}$ ,  $\mathbf{C}$  is the right Cauchy-Green deformation tensor,  $\mu_m$  is the shear modulus of the ground matrix,  $\mathbf{I}$  is the identity tensor, and  $C_{33} = 1/(C_{11}C_{22} - C_{12}^2)$  results from the incompressibility constraint.<sup>13</sup> The effective fiber ensemble response was modeled as

$$S_{\text{ens}}(E_{\text{ens}}) = \begin{cases} c_0 (e^{c_1 E_{\text{ens}}} - 1) & \forall E_{\text{ens}} \leq E_{\text{ub}} \\ c_0 (e^{c_1 E_{\text{ub}}} - 1) + c_0 c_1 e^{c_1 E_{\text{ub}}} (E_{\text{ens}} - E_{\text{ub}}) & \forall E_{\text{ens}} > E_{\text{ub}}, \end{cases} \quad (2)$$

where  $c_0$  and  $c_1$  are material constants and  $E_{ub}$  is the upper bound strain for collagen fiber recruitment; beyond  $E_{ub}$ ,  $S_{ens}$  is linear with respect to  $E_{ens}$ . Circumferential and radial directions were defined as detailed in Rego *et al.*<sup>33</sup> Values for the material parameters used in the material model have been published previously<sup>33</sup> and are summarized in Table 1. The complete constitutive model was implemented in an Abaqus Explicit subroutine (VUMAT) for FE simulations.

The boundary and loading conditions used in the simulations are summarized below (Fig. 2). An annular displacement boundary condition was determined using the geometries extracted from the open and closed MV states in each image (Fig. S1). We assumed a uniform percent change across the entire circumference of the annulus. A uniform 100mmHg pressure was applied to the ventricular surface of the MV leaflets and a downward chordal mimicking force (CMF) to the free edge. Finally, a local corrective pressure field (LCPF) was enforced to more closely match the local shape variations of the closed MV leaflets. The LCPF applies pressure linearly proportional to the distance of the MV leaflet from the true closed state geometry and updates at each time step.

### Post-processing

To average computed quantities across several valves, the computed strain fields were re-expressed in a 2D parametric space that allowed for direct correspondence of material points between meshes (Fig. 3). As described previously,<sup>31</sup> a conformal map was generated by solving the Laplace equation with Dirichlet conditions at the MV annulus and free edge and assigned to each triangulated MV mesh. This map preserves orthogonality between the radial and circumferential material directions and allows for a direct comparison for locally correspondent values of strain between valves. A grid resolution of approximately 3 points per mm was used in order to approximately match the feature resolution on the leaflet surface. In the re-parameterized values, we systematically defined leaflet segments according to Carpentier's nomenclature (anterior segments A1–3, posterior segments P1–3) and statistically compared these segments between groups of valves. Additionally, shear strains were computed: the shear angle  $\alpha$  was defined as the deviation of the angle from 90° between circumferential and radial material directions during MV closure. Shear angle was calculated locally across the MV leaflets and averaged within each group of valves.

### Statistical Analysis

To numerically determine differences between groups of MVs, we performed two-tailed Student's t-tests to compare dimensional metrics including leaflet area, annular length, and effective orifice area in the MVs before and after surgery. Similarly, we compared average strain in the commissural segments of the MV as well as in the mid-leaflet segments. Circumferential and radial strains were averaged across all grid points within each leaflet region of the MV in each individual and then statistically compared between MVs with recurrent and non-recurrent IMR, and between MVs with IMR and healthy or “normal” MVs. A  $p$ -value of  $<0.05$  was considered significant for all t-tests. Anderson-Darling tests were performed prior to each t-test, none of which rejected normality.

To quantify the ability of the data to predict 6-month outcomes, we first fit a logistic regression model to the averaged leaflet strains in segments where we had found a statistical difference between absence or presence of recurrence of MR 6 months post-surgery from a two-sample t-test. We then fit a receiver operating characteristic (ROC) curve to this data and found an optimal area under the curve (AUC) and cutoff value to quantify the quality of the available data as a predictive model. A higher AUC corresponds to a better prediction of 6-month patient outcomes, or a high ratio of accurately identified 6-month outcome to inaccurately identified outcome.

## RESULTS

### MV Leaflet Deformation Patterns

We observed clear variations between individual MV, including a trend toward IMR MV being larger than those without IMR, and recurrent MV being larger than non-recurrent MV. We averaged the pre-surgical directional strains and mapped them onto their respective averaged 3D valve geometries for each group of MVs (Fig. 4). The deformation of the anterior and posterior leaflets was markedly different, with extensional circumferential strain found only in the central region of the anterior leaflet and not the posterior leaflet. The pattern of circumferential strain was also visibly different between groups, and post-IMR MVs tended to have lower magnitudes of circumferential strain in both leaflets than the normal MVs. There was also significantly higher radial strain in the MV leaflets with IMR. An example of circumferential and radial strains for a representative non-recurrent MV is included in the supplemental material (Fig. S2).

A two-tailed Student's t-test at each commissure and mid-leaflet region of the non-recurrent and recurrent groups found a statistically significant difference ( $p = 0.0223$ ) in average circumferential strain at the anterior commissure (Carpentier segments A1 and P1) between the recurrent and non-recurrent valves (Fig. 5). Comparing average strains in individual segments between the two groups results showed statistically different circumferential strains in the A1 segment of the MVs in the pre-surgical state, with a  $p$ -value of 0.0186. These marked distinctions in leaflet strain indicate different patterns of deformation in the groups, with non-recurrent MV commissures compressing substantially more than recurrent MV commissures, and may be caused by a difference between infarct location in the LVs of each group or different states of disease progression.

### Shear Strain

Leaflet shear strain of appreciable magnitude was found mainly in the anterior leaflets, concentrated near the commissures for both normal MVs and MVs with IMR in the pre-surgical state. Each group showed similar patterns of positive and negative shear in the anterior leaflet (Fig. 6). There were much higher magnitudes of shear in the posterior leaflet segments of the normal MVs than in those of MVs with IMR. This trend is similar to that found by Rego *et al.* in the ovine MV from pre- to post-MI<sup>31</sup>: as time passes after the onset of MI, the magnitude of shear in the posterior ovine MV leaflet goes down to nearly 0. The trend indicates that there may be a correlation between shear strain pattern and degree of disease progression in human MVs.

## Further Statistical Analyses

A logistic regression model for the average pre-surgical circumferential strain in the A1 segment of the recurrent and non-recurrent valves also showed statistical difference between the two groups with a  $p$ -value of 0.0362 (Fig. 7). A receiver operating characteristic (ROC) curve for averaged pre-surgical circumferential A1 segment strains had a high area under the curve (AUC) of 0.832 with a cutoff strain of  $-0.18$  (Fig. 7), indicating that average pre-surgical circumferential strains in the A1 segment were independently able to accurately predict whether a valve will have MR recurrence at 6 months post-surgery with an accuracy of 83.2%, and that an average strain below  $-0.18$  is likely to be associated with a MV without recurrence of MR at 6 months.

## General Geometric Characteristics

In addition to the in-plane deformation patterns, we also examined the averaged 2D representations of the MVs and computed dimensional metrics (Fig. S3 and Table S1) demonstrated again that the MV leaflets and annuli were significantly larger in post-IMR MVs than in normal MVs, and were larger in valves that later had repair failure than in those which later underwent a successful repair. There was little difference in the MV orifice area in the post-surgical state of the non-recurrent and recurrent groups, and both were smaller than the normal MVs, as expected from the undersized nature of the rings used in URA. The leaflet area and annular length of normal MVs was significantly smaller than those of the pre-surgical non-recurrent MVs ( $p = 0.0290$ ,  $p = 0.0410$ ) and of the recurrent MVs ( $p = 0.0047$ ,  $p = 0.0099$ ), corresponding to LV dilation that occurs in IMR. The undersized rings used in repair surgery lead orifice areas in both the non-recurrent and recurrent groups to be significantly smaller than the average orifice area of the normal MVs ( $p = 0.0037$  and  $0.0096$  respectively). A comparison of these computed geometric characteristics to those of the larger data set from which they were obtained shows that they fall within the expected ranges and that the data in this study was representative of the larger population.<sup>6</sup>

## DISCUSSION

### Study Overview and Key Findings

Overview Many years of research into the mechanisms of the onset and progression of IMR have brought to light its very complex nature, and thus the necessity of a thorough understanding of the progression of the disease for optimal treatment. These complexities range from the large-scale kinematic changes that occur in IMR due to the dilation of the LV to changes in the genetic expression in mitral valve interstitial cells (MVICs).<sup>4,5</sup> The use of computational modeling has proven to be an effective approach to evaluate the response of the MV both post-MI and after repair to gain unique insights into the underlying mechanisms of functional MV disease.<sup>35</sup> Importantly, improvements in imaging technologies have allowed us to study these changes in a completely non-invasive manner *in vivo* so as to observe the MV/LV system and be able to track these changes over time. In the present study, we directly utilized clinical data to build patient-specific, 3D geometric models of each MV studied in the fully opened and fully closed states. This allowed us to compare MV leaflet deformations in groups with successful post-repair outcomes to those with recurrence of

IMR. These novel findings yielded pre-surgical insights for fundamental understanding of the MV in IMR.

**Key findings** Our analyses determined that patterns of MV leaflet strain, while complex, consistently displayed statistical differences between the recurrent and non-recurrent groups, especially in the commissural segments. Specifically, we found that the normal MVs had significantly greater compressive circumferential strain in the posterior MV leaflet and significantly lower radial strain in both MV leaflets, corresponding to an increased ability of the annulus to contract fully and less downward tethering of the MV leaflets respectively. Circumferential pre-surgical strain in particular was found to be statistically different between the recurrent and non-recurrent groups of valves, especially at the anterior commissure. These differences in leaflet strain indicated that there is a clear difference in the deformation of the leaflets between the two groups during systole. In particular, the tissue near the commissures of the non-recurrent valves compresses more circumferentially than that of the recurrent valves. The difference in kinematics may be affected by the manifestation of the infarct in the LV, as an infarct closer to the annulus would be likely to lead to less annular contraction and thus lower circumferential compressive strain in the recurrent valves. It may also be caused by an effective stiffening of the MV due to plastic deformations.<sup>31</sup> In order to fully understand how this difference manifests during MV closure and how the MV interacts with the infarcted LV, it is necessary to have a full model of the MV.

Not surprisingly, we found no statistically significant differences in circumferential or radial leaflet strains between the recurrent and non-recurrent MV groups immediately post-surgery. The lack of statistical difference may occur because the URA procedure forces the MV annuli of all MVs into a similar size and shape. However, this does not imply that there is no difference in the stress states of these groups. There may be some true differences in strain between groups which could be elucidated by using a larger sample size. We are also limited by the technique used for the study, as it only allows us to study leaflet strains and not tissue stresses or interaction with the larger MV/LV system. In order to look at these other aspects of the complex MV system, it is necessary to build full models with physically realistic constraints, as those developed by Drach *et al.*<sup>12</sup> and Khalighi *et al.*<sup>18</sup>

An analysis of shear strain showed that the posterior leaflets of the normal MVs clearly underwent shear deformation, while the MVs with IMR had negligible shear in the posterior leaflet. This trend matches that found in the ovine MV, where shear deformation in the posterior MV leaflet became negligible within 8 weeks after the onset of IMR and was greatest in the commissural segments of the anterior leaflet.<sup>31</sup> The most progressed state of IMR studied in the ovine MVs had a pattern of shear similar to that in MVs of patients with moderate-severe to severe IMR, suggesting that the pattern of shear in the MV leaflets may be correlated with the degree of disease progression in a patient. While these differences were not found to be statistically significant, they should be studied further using a larger data set.

We found that on average, the recurrent MVs were larger than the non-recurrent MVs, and both groups of valves with IMR were larger than the normal MVs. These differences in size



may be indicative of differences in the degree of IMR progression, where the progression of IMR leads to larger MVs that have undergone plastic changes and are more difficult to repair. As discussed by Rego *et al.*,<sup>31</sup> a more progressed disease state in the ovine MV is associated with reduced annular contraction. The condition is similar in humans: as IMR progresses, the LV progressively dilates and the loss of contractile function in the infarct region prevents the LV from constricting enough to allow the MV annulus to fully contract and the MV to close. While the open MVs in the recurrent and non-recurrent groups have similar annular characteristics, the closed valves have significantly different annular dimensions, suggesting that the recurrent MV annuli contracted less. This difference between the groups may also be related to the location of the infarct in the LV, as an infarct closer to the annulus would prevent annular contraction to a greater degree. Furthermore, the higher leaflet area in the recurrent valves in both open and closed pre-surgical states may be associated with increased or prolonged downward tethering. Prolonged excessive stretching is believed to lead to permanent changes in the open/reference state of the MV structure and is associated with changes in the diastolic degree of stretch in the collagen as well as apparent stiffening of the tissue. Such altered leaflet loading is also closely linked to changes in MVIC deformation, and this abnormal MVIC loading has been found to lead to altered remodeling and levels of expression of extracellular matrix (ECM) components.<sup>5,19,23,34,39</sup> The associated changes in tissue mechanical properties may affect the success or failure of a repair surgery, indicating a need to better the etiology of the disease and its progression.

Similar to post-surgical strains, we found no statistical difference in post-surgical geometric characteristics such as leaflet and annulus size between recurrent and non-recurrent MVs. Meijerink *et al.* recently analyzed post-surgical data from the patients originally studied by Bouma *et al.* and found the same result: post-surgical geometric characteristics such as annular dimensions and tethering angle were not significantly different between recurrent and non-recurrent MVs.<sup>6,25</sup>

### Insights into MV Responses to IMR and Annuloplasty Surgery

Our key findings from this study, consistent with our understanding from ovine IMR models, confirm that the human post-IMR MV is in a substantially altered state compared to normal. The dilation of the LV caused by chronic ischemic conditions restrict the MV from deforming in the same way as a healthy MV. Howsmon *et al.* recently found in an ovine model that genes involved in extracellular matrix organization were downregulated at four weeks after the onset of a MI but returned to baseline by eight weeks post-MI.<sup>16</sup> This suggests that the tissue responds at the cellular level to altered loading conditions, increasing collagen mass fraction and decreasing levels of glycosaminoglycan expression to prevent tissue damage, but settles over time to a new homeostatic state. Thus, abnormal deformation patterns produce a result consistent with a plastic tissue response. It is thus expected that human MV will respond similarly to ischemic conditions. Previous studies have observed plastic deformation in the MV and discussed how to identify it in clinical images.<sup>41,3</sup> Our findings are consistent with the observation that human MVs do indeed undergo plastic changes in IMR, as we found that the leaflets of MVs with IMR tended to be much longer than those without IMR. In addition to this, we have elucidated the changes in local strain

and deformation that occur after the onset of IMR, extending our understanding of the disease in humans and confirming the complexity of the condition.

### Limitations

While comprehensive, the available clinical data only included images from immediately prior to and after surgery, and did not include any information about the MV prior to the onset of IMR or beyond the 6-month time point. We are thus unable to track changes in individual MVs over extended periods of time to better understand either the progression of IMR in humans or to observe the changes that occur in a patient's MV in the months following repair surgery. Additionally, while we found several key statistical differences in deformation patterns and size between the recurrent and non-recurrent MVs, our sample size was limited in size and exclusively focused on IMR patient data. Thus, our findings may not completely represent the effects of other MV prolapse mechanisms, such as 'organic' (e.g. myxomatous) mitral regurgitation. That said, the present study clearly provided insights into MV functionality, and thus established guidelines for other mitral valve pathologies in larger population-wide studies. Finally, we note that the noninvasive image-based strain estimation method was not able to provide information about leaflet stresses, which will affect leaflet tissue remodeling. It also does not capture the complete interaction of the MV and LV and cannot show how LV remodeling in IMR affects the function of the MV. Future studies will work toward the development of full MV models with physically realistic constraints that are able to provide even more information about the behavior of the MV tissue as well as combined models of the MV and LV to elucidate how functional changes in the larger system affect MV mechanics.

### Translational Implications

In the present study, we determined that there were substantial, observable differences in the state of the MV between valves that have successful MV repair *via* URA and those with failure of the repair and thus recurrence of MR at 6 months post-surgery. By extending the work of Bouma *et al.*,<sup>6</sup> we have found that surgical outcomes are associated with quantifiable differences in the kinematic state of the MV and IMR prior to surgery, making it likely that such pre-surgical differences could be used to predict the outcome of a repair procedure. These quantifiable metrics were derived directly from routinely acquired rt-3DE images, making a method like ours more straightforward to implement in the clinical decision-making process. Future studies will use the same kind of clinical imaging data to work toward the development of full human MV models with functionally equivalent chordae tendinae and the implementation of these models into a model involving the LV. Such models will help us develop a broader understanding of local tissue stresses, MV kinematics during closure, and the interaction of the full MV/LV system. In doing so, we hope to elucidate how the infarcted LV combined with various methods of repair affect MV kinematics and how this then affects the longer-term plastic changes, growth, and remodeling observed in MV tissue. Such robust, patient-specific models could help quantify the efficacy of surgical repair through computer simulations, improve clinical assessments, and thereby optimize surgical repair of the MV.

## Supplementary Material

Refer to Web version on PubMed Central for supplementary material.

## ACKNOWLEDGEMENTS

This work was supported by the National Heart, Lung and Blood Institute of the National Institutes of Health (R01-HL119297 to J.H.G. and M.S.S., R01-HL73021 and R01-HL63954 to R.C.G. and J.H.G.); the American Heart Association (18PRE34030258 to B.V.R.); the National Science Foundation (DGE-1610403 to B.V.R.); the Harry S. Moss Heart Trust; and the Cain Foundation-Seton-Dell Medical School Endowment for Collaborative Research.

## ABBREVIATIONS

<b>AA</b>	Anterior mitral annulus
<b>AC</b>	Anterior commissure
<b>AML</b>	Anterior mitral leaflet
<b>AUC</b>	Area under curve
<b>AoV</b>	Aortic valve
<b>CMF</b>	Chordal mimicking force
<b>ED</b>	End diastole
<b>ES</b>	End systole
<b>FE</b>	Finite element
<b>IMR</b>	Ischemic mitral regurgitation
<b>LA</b>	Left atrium
<b>LCPF</b>	Local corrective pressure field
<b>LFE</b>	Leaflet free edge
<b>LV</b>	Left ventricle
<b>LVOT</b>	Left ventricular outflow tract
<b>MI</b>	Myocardial infarction
<b>MR</b>	Mitral regurgitation
<b>MV</b>	Mitral valve
<b>MVIC</b>	Mitral valve interstitial cell
<b>PA</b>	Posterior mitral annulus
<b>PC</b>	Posterior commissure
<b>PM</b>	Papillary muscle

<b>PML</b>	Posterior mitral leaflet
<b>rt-3DE</b>	Real-time 3D echocardiography
<b>URA</b>	Undersized ring annuloplasty

## REFERENCES

1. Acker MA, Parides MK, Perrault LP, Moskowitz AJ, Gelijns AC, Voisine P, Smith PK, Hung JW, Blackstone EH, Puskas JD, et al. Mitral-valve repair versus replacement for severe ischemic mitral regurgitation. *N Engl J Med* 370(1):23–32, 2014. [PubMed: 24245543]
2. Alfieri O, Maisano F, De Bonis M, Stefano PL, Torracca L, Oppizzi M, and La Canna G. The double-orifice technique in mitral valve repair: a simple solution for complex problems. *J Thorac Cardiovasc Surg* 122(4):674–681, 2001. [PubMed: 11581597]
3. Avila Vanzini N, Michelena HI, Fritche Salazar JF, Herrera Bello H, Siu Moguel S, Rodriguez Ocampo RR, Oregel Camacho DJ, and Espinola Zavaleta N. Clinical and echocardiographic factors associated with mitral plasticity in patients with chronic inferior myocardial infarction. *Eur Heart J Cardiovasc Imaging* 19(5):508–515, 2018. [PubMed: 29529256]
4. Ayoub S, Howsmon DP, Lee C-H, and Sacks MS. On the role of predicted in vivo mitral valve interstitial cell deformation on its biosynthetic behavior. *Biomech Model Mechanobiol* 20:135–144, 2021. [PubMed: 32761471]
5. Ayoub S, Lee C-H, Driesbaugh KH, Anselmo W, Hughes CT, Ferrari G, Gorman RC, Gorman JH, and Sacks MS. Regulation of valve interstitial cell homeostasis by mechanical deformation: implications for heart valve disease and surgical repair. *J R Soc Interface* 14(135):20170580, 2017. [PubMed: 29046338]
6. Bouma W, Lai EK, Levack MM, Shang EK, Pouch AM, Eperjesi TJ, Plappert TJ, Yushkevich PA, Mariani MA, Khabbaz KR, et al. Preoperative three-dimensional valve analysis predicts recurrent ischemic mitral regurgitation after mitral annuloplasty. *Ann Thorac Surg* 101(2):567–575, 2016. [PubMed: 26688087]
7. Chan V, Chen L, Mesana L, Mesana TG, and Ruel M. Heart valve prosthesis selection in patients with endstage renal disease requiring dialysis: a systematic review and meta-analysis. *Heart* 97(24):2033–2037, 2011. [PubMed: 21990382]
8. Chaput M, Handschumacher MD, Guerrero JL, Holmvang G, Dal-Bianco JP, Sullivan S, Vlahakes GJ, Hung J, Levine RA, and Leducq Foundation MITRAL Transatlantic Network. Mitral leaflet adaptation to ventricular remodeling: prospective changes in a model of ischemic mitral regurgitation. *Circulation* 120(11 Suppl):S99–103, 2009. [PubMed: 19752393]
9. Dal-Bianco JP, and Levine RA. Anatomy of the mitral valve apparatus: role of 2D and 3D echocardiography. *Cardiol Clin* 31(2):151–164, 2013. [PubMed: 23743068]
10. De Bonis M, and Alfieri O. Mitral regurgitation should be corrected in patients with dilated cardiomyopathy. *Nat Clin Pract Cardiovasc Med* 5(8):452–453, 2008. [PubMed: 18560405]
11. Di Salvo TG, Acker MA, Dec GW, and Byrne JG. Mitral valve surgery in advanced heart failure. *J Am Coll Cardiol* 55(4):271–282, 2010. [PubMed: 20117430]
12. Drach A, Khalighi AH, and Sacks MS. A comprehensive pipeline for multiresolution modeling of the mitral valve: validation, computational efficiency, and predictive capability. *Int J Numer Method Biomed Eng* 2018. 10.1002/cnm.2921.
13. Fan R, and Sacks MS. Simulation of planar soft tissues using a structural constitutive model: finite element implementation and validation. *J Biomech* 47(9):2043–2054, 2014. [PubMed: 24746842]
14. Feldman T, Kar S, Rinaldi M, Fail P, Hermiller J, Smalling R, Whitlow PL, Gray W, Low R, Herrmann HC, et al. Percutaneous mitral repair with the MitraClip system: safety and midterm durability in the initial EVEREST (Endovascular Valve Edge-to-Edge REpair Study) cohort. *J Am Coll Cardiol* 54(8):686–694, 2009. [PubMed: 19679246]
15. Goldstein D, Moskowitz AJ, Gelijns AC, Ailawadi G, Parides MK, Perrault LP, Hung JW, Voisine P, Dagenais F, Gillinov AM, et al. Two-year outcomes of surgical treatment of severe ischemic mitral regurgitation. *N Engl J Med* 374(4):344–353, 2016. [PubMed: 26550689]

16. Howsmon DP, Rego BV, Castellero E, Ayoub S, Khalighi AH, Gorman RC, Gorman JH, Ferrari G, and Sacks MS. Mitral valve leaflet response to ischaemic mitral regurgitation: from gene expression to tissue remodelling. *J R Soc Interface* 17(166):20200098, 2020. [PubMed: 32370692]
17. Khalighi AH, Drach A, Gorman RC, Gorman JH, and Sacks MS. Multiresolution geometric modeling of the mitral heart valve leaflets. *Biomech Model Mechanobiol* 17(2):351–366, 2018. [PubMed: 28983742]
18. Khalighi AH, Rego BV, Drach A, Gorman RC, Gorman JH, and Sacks MS. Development of a functionally equivalent model of the mitral valve chordae tendineae through topology optimization. *Ann Biomed Eng* 47(1):60–74, 2019. [PubMed: 30187238]
19. Khang A, Buchanan RM, Ayoub S, Rego BV, Lee C-H, Ferrari G, Anseth KS, and Sacks MS. Mechanobiology of the heart valve interstitial cell: Simulation, experiment, and discovery. In: *Mechanobiology in health and disease*, edited by Verbruggen SW. London: Elsevier, 2018.
20. Kuwahara E, Otsuji Y, Iguro Y, Ueno T, Zhu F, Mizukami N, Kubota K, Nakashiki K, Yuasa T, Yu B, et al. Mechanism of recurrent/persistent ischemic/functional mitral regurgitation in the chronic phase after surgical annuloplasty: importance of augmented posterior leaflet tethering. *Circulation* 114(1 Suppl):I529–534, 2006. [PubMed: 16820632]
21. Laniado S, Yellin EL, Miller H, and Frater RW. Temporal relation of the first heart sound to closure of the mitral valve. *Circulation* 47(5):1006–1014, 1973. [PubMed: 4705568]
22. Lee C-H, Rabbah J-P, Yoganathan AP, Gorman RC, Gorman JH, and Sacks MS. On the effects of leaflet microstructure and constitutive model on the closing behavior of the mitral valve. *Biomech Model Mechanobiol* 14(6):1281–1302, 2015. [PubMed: 25947879]
23. Lee C-H, Zhang W, Feaver K, Gorman RC, Gorman JH, and Sacks MS. On the in vivo function of the mitral heart valve leaflet: insights into tissue-interstitial cell biomechanical coupling. *Biomech Model Mechanobiol* 16(5):1613–1632, 2017. [PubMed: 28429161]
24. Lorusso R, Gelsomino S, Vizzardi E, D'Aloia A, De Cicco G, Luca F, Parise O, Gensini GF, Stefano P, Livi U, et al. Mitral valve repair or replacement for ischemic mitral regurgitation? The Italian study on the treatment of ischemic mitral regurgitation (ISTIMIR). *J Thorac Cardiovasc Surg* 145(1):128–139, 2013. [PubMed: 23127376]
25. Meijerink F, Wijdhen Hamer IJ, Bouma W, Pouch AM, Aly AH, Lai EK, Eperjesi TJ, Acker MA, Yushkevich PA, Hung J, et al. Intraoperative postannuloplasty three-dimensional valve analysis does not predict recurrent ischemic mitral regurgitation. *J Cardiothorac Surg* 15(1):161, 2020. [PubMed: 32616001]
26. Messas E, Guerrero JL, Handschumacher MD, Conrad C, Chow CM, Sullivan S, Yoganathan AP, and Levine RA. Chordal cutting: a new therapeutic approach for ischemic mitral regurgitation. *Circulation* 104(16):1958–1963, 2001. [PubMed: 11602501]
27. Michler RE, Smith PK, Parides MK, Ailawadi G, Thourani V, Moskowitz AJ, Acker MA, Hung JW, Chang HL, Perrault LP, et al. Two-year outcomes of surgical treatment of moderate ischemic mitral regurgitation. *N Engl J Med* 374(20):1932–1941, 2016. [PubMed: 27040451]
28. Mihos CG, Capoulade R, Yucel E, Melnitchouk S, and Hung J. Combined papillary muscle sling and ring annuloplasty for moderate-to-severe secondary mitral regurgitation. *J Card Surg* 31(11):664–671, 2016. [PubMed: 27620350]
29. Nkomo VT, Gardin JM, Skelton TN, Gottdiener JS, Scott CG, and Enriquez-Sarano M. Burden of valvular heart diseases: a population-based study. *Lancet* 368(9540):1005–1011, 2006. [PubMed: 16980116]
30. Perrault LP, Moskowitz AJ, Kron IL, Acker MA, Miller MA, Horvath KA, Thourani VH, Argenziano M, D'Alessandro DA, Blackstone EH, et al. Optimal surgical management of severe ischemic mitral regurgitation: to repair or to replace? *J Thorac Cardiovasc Surg* 143(6):1396–1403, 2012. [PubMed: 22054660]
31. Rego BV. Remodeling of the mitral valve: an integrated approach for predicting long-term outcomes in disease and repair. Ph.D. thesis, The University of Texas at Austin, 2019.
32. Rego BV, Ayoub S, Khalighi AH, Drach A, Gorman JH, Gorman RC, and Sacks MS. Alterations in mechanical properties and in vivo geometry of the mitral valve following myocardial infarction. In *SB3C 2017 Proceedings*, pp. SB3C2017–1. 2017.

33. Rego BV, Khalighi AH, Drach A, Lai EK, Pouch AM, Gorman RC, Gorman JH, and Sacks MS. A noninvasive method for the determination of in vivo mitral valve leaflet strains. *Int J Numer Method Biomed Eng* 34(12):2018.
34. Rego BV, Wells SM, Lee C-H, and Sacks MS. Mitral valve leaflet remodelling during pregnancy: insights into cell-mediated recovery of tissue homeostasis. *J R Soc Interface* 13(125):20160709, 2016. [PubMed: 27928033]
35. Sacks MS, Drach A, Lee C-H, Khalighi AH, Rego BV, Zhang W, Ayoub S, Yoganathan AP, Gorman RC, and Gorman JH. On the simulation of mitral valve function in health, disease, and treatment. *J Biomech Eng* 141(7):0708041–07080422, 2019.
36. Sacks MS, Enomoto Y, Graybill JR, Merryman WD, Zeeshan A, Yoganathan AP, Levy RJ, Gorman RC, and Gorman JH. In-vivo dynamic deformation of the mitral valve anterior leaflet. *Ann Thorac Surg* 82(4):1369–1377, 2006. [PubMed: 16996935]
37. Sacks MS, He Z, Baijens L, Wanant S, Shah P, Sugimoto H, and Yoganathan AP. Surface strains in the anterior leaflet of the functioning mitral valve. *Ann Biomed Eng* 30(10):1281–1290, 2002. [PubMed: 12540204]
38. Sacks MS, Khalighi A, Rego B, Ayoub S, and Drach A. On the need for multi-scale geometric modelling of the mitral heart valve. *Healthc Technol Lett* 4(5):150–150, 2017. [PubMed: 29184654]
39. Sacks M, Rego B, Howsmon D, and Wells S. What is the remodeling potential of the native heart valve? *Struct Heart* 4(sup1):45–45, 2020.
40. Takeda K, Sakaguchi T, Miyagawa S, Shudo Y, Kainuma S, Masai T, Taniguchi K, and Sawa Y. The extent of early left ventricular reverse remodelling is related to midterm outcomes after restrictive mitral annuloplasty in patients with non-ischaemic dilated cardiomyopathy and functional mitral regurgitation. *Eur J Cardiothorac Surg* 41(3):506–511, 2012. [PubMed: 22011774]
41. Topilsky Y Mitral plasticity: possible target for intervention in patients with ischaemic mitral regurgitation? *Eur Heart J Cardiovasc Imaging* 19(5):501–502, 2018. [PubMed: 29529174]

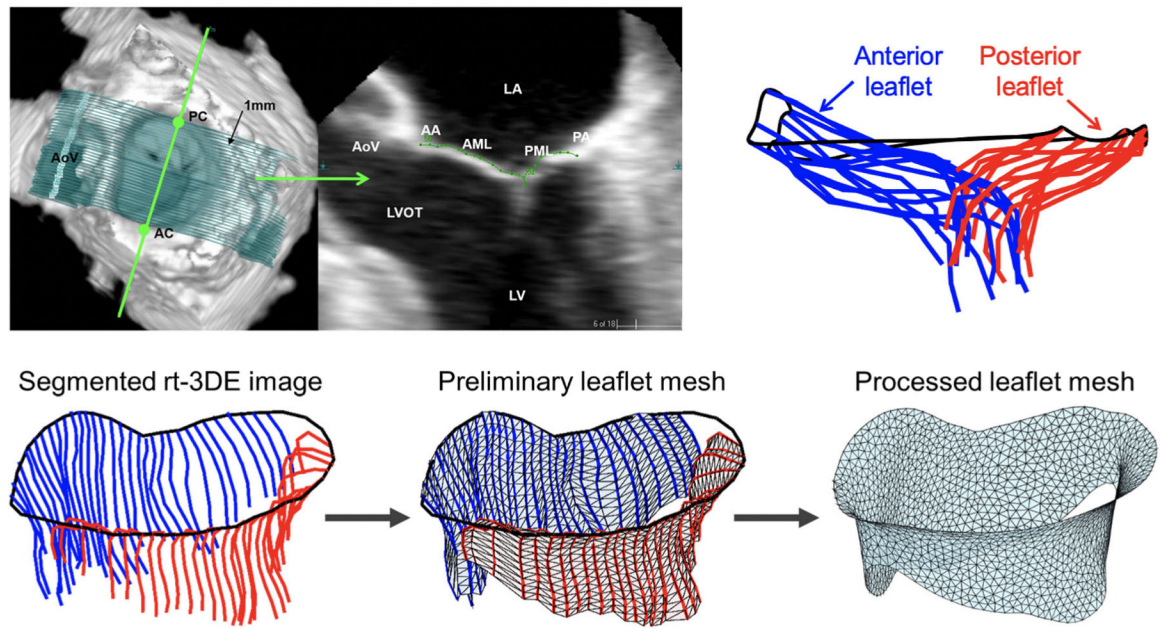
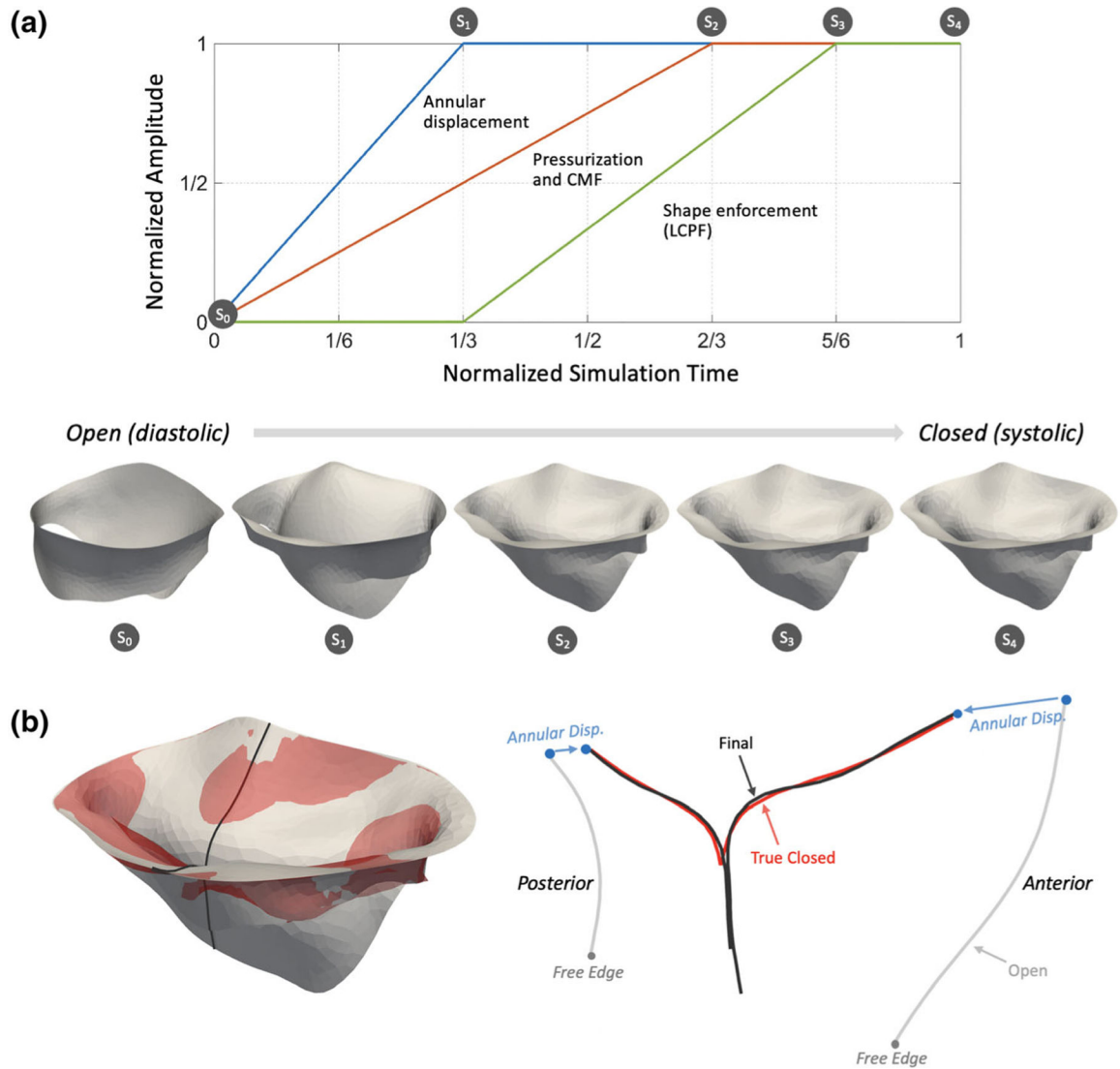
**FIGURE 1.**

Image segmentation and mesh generation pipeline. Noninvasive rt-3DE images were traced at several short-axis cross-sections approximately 1mm apart along the intercommissural length (top), and patient-specific FE meshes were generated from the image traces using surface triangulation, sampling, reconstruction, and smoothing algorithms (bottom). Adapted from Rego *et al.*<sup>31</sup> *AA* anterior mitral annulus, *AC* anterior commissure, *AML* anterior mitral leaflet, *AoV* aortic valve, *LA* left atrium, *LV* left ventricle, *LVOT* left ventricular outflow tract, *PA* posterior mitral annulus, *PC* posterior commissure, *PML* posterior mitral leaflet.



**FIGURE 2.**

An overview of the FE simulation used to morph the open state MV mesh into the closed shape. (a) The time course over which each of the loading and boundary conditions were applied.  $S_{0-4}$  show the shape of the MV at several points, namely at the open state of the valve, after each boundary and loading condition is fully applied, and at the end of the simulation. (b) At the left, the true segmented geometry of the closed valve (red) is overlaid with the closed morphed valve geometry (grey). The figure on the right shows the cross-section of the valve at the center of the geometry and shows a close match between the segmented and morphed geometries.



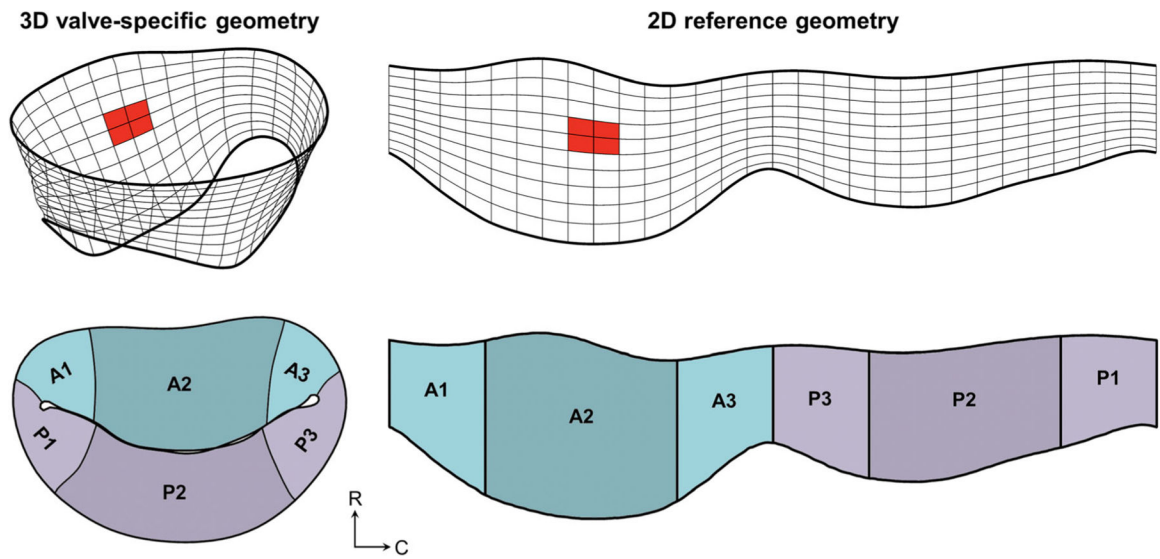


**FIGURE 3.** The 3D geometry of each MV was remapped to a 2D representation and assigned an interpolated rectangular grid with spatial resolution of approximately 3 points per mm. The segments A1–3 and P1–3 were defined as shown, where the anterior leaflet is shaded in blue and the posterior leaflet is shaded in purple.

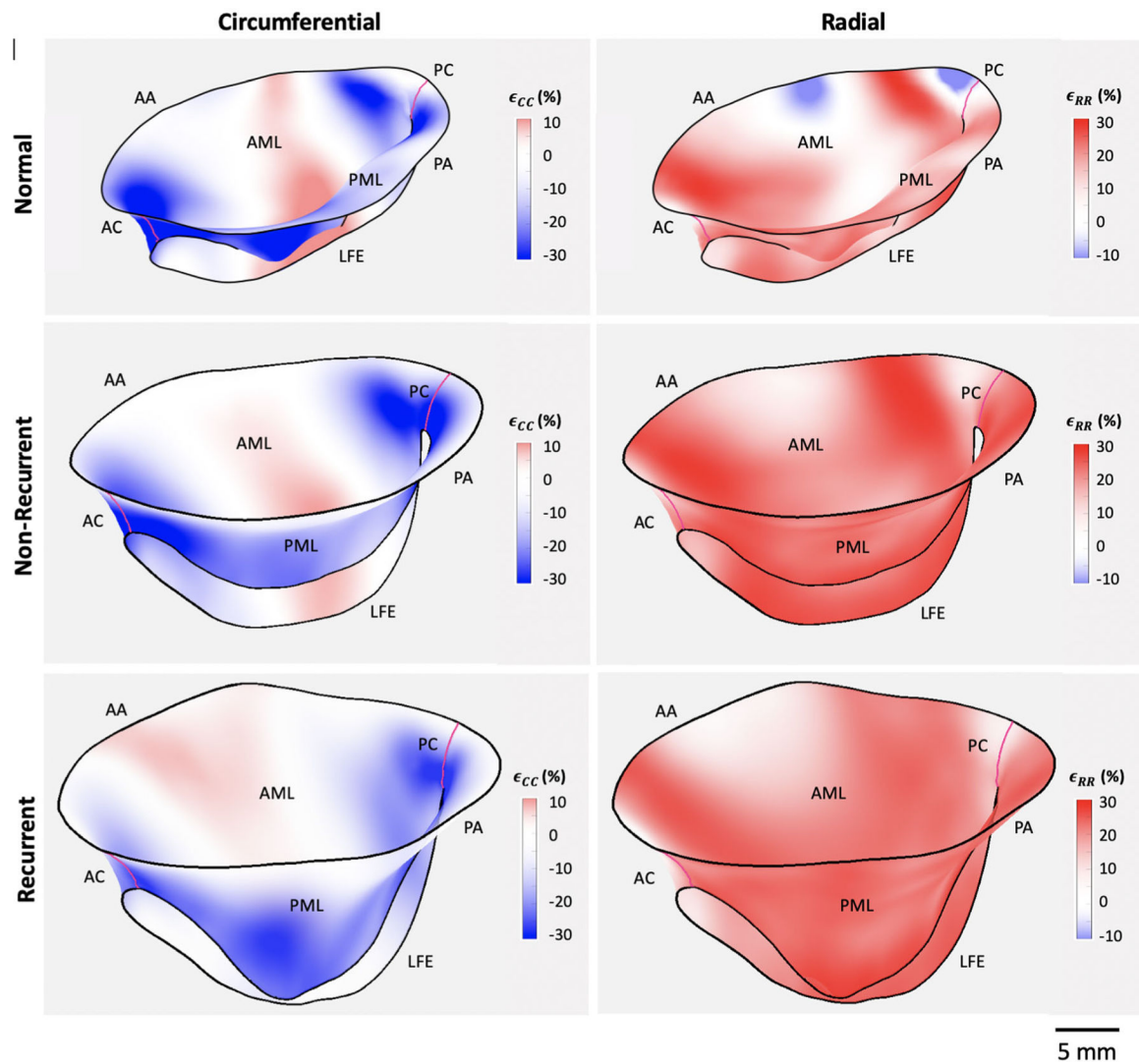


**FIGURE 4.**

Average directional strains plotted on the corresponding averaged 3D geometries for the groups of MVs without IMR and with non-recurrent and recurrent MR. There is a trend toward compressive circumferential strain at the commissures and tensile circumferential strain toward the center of the anterior leaflet. The recurrent MVs are larger on average than the non-recurrent MVs, which tend to be larger than MVs without IMR. *AA* anterior mitral annulus, *AC* anterior commissure, *AML* anterior mitral leaflet, *LFE* leaflet free edge, *PA* posterior mitral annulus, *PC* posterior commissure, *PML* posterior mitral leaflet.

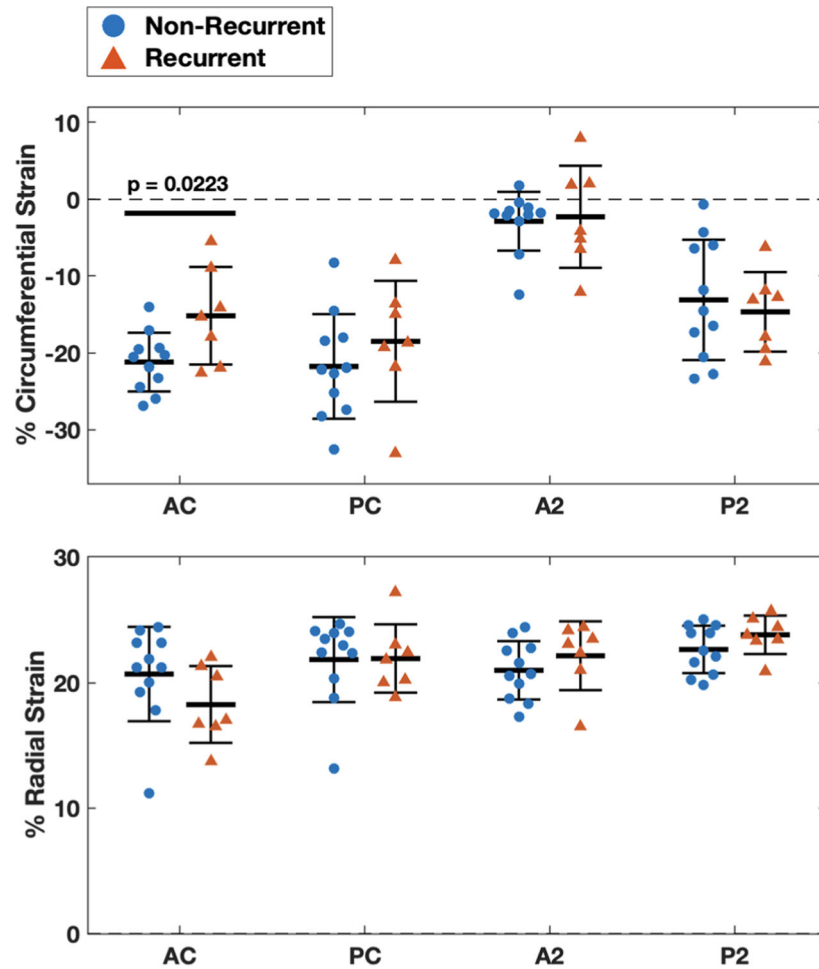


**FIGURE 5.** Averaged circumferential and radial strains in functional MV leaflet segments for individual non-recurrent and recurrent MVs and associated means  $\pm$  standard deviations. The charts show strains averaged at the anterior commissure (AC, Carpentier segments A1 and P1) and posterior commissure (PC, Carpentier segments A3 and P3) and each mid-leaflet segment separately. The average circumferential strain at the anterior commissure is significantly different between the non-recurrent and recurrent MVs as determined by a two-tailed Student's *t*-test ( $p = 0.0223$ ). There is no significant difference in averaged circumferential strain in the PC, A2 and P2 regions, or in radial strain between the recurrent and non-recurrent groups.

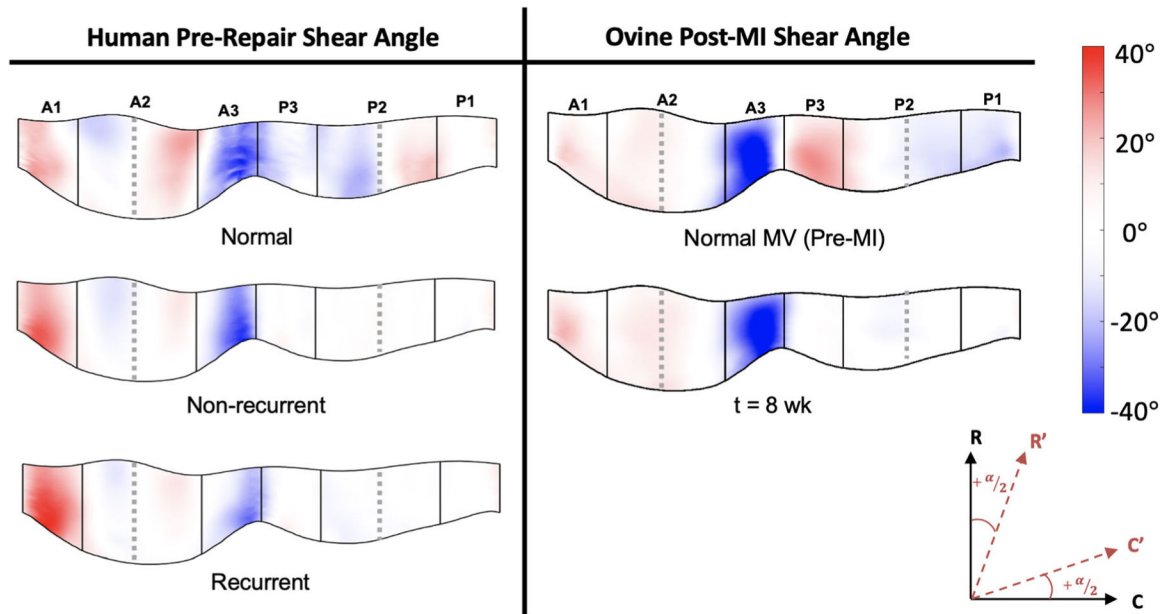


**FIGURE 6.**

Locally averaged shear angle in human and ovine MVs with severe MR prior to surgical repair, calculated as the change in the closed state of the valve from the open state. The spatial distribution of shear in the human MVs with IMR prior to surgery is comparable to that in ovine MV leaflets with IMR several weeks after an MI. There is no statistical difference in shear angle between the non-recurrent and recurrent human MVs.

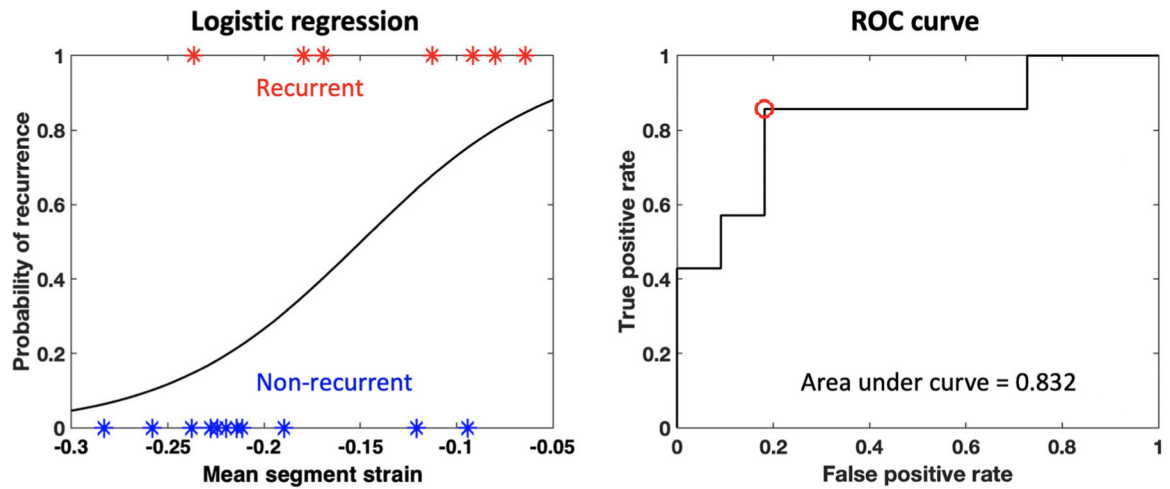


**FIGURE 7.**

Logistic regression curve (left) and ROC curve (right) using segment-averaged pre-surgical circumferential strains in the A1 segment for individual valves. Logistic regression found a significant difference between strain for non-recurrent and recurrent valves ( $p = 0.0362$ ). The ROC curve had a high AUC (0.832), indicating that average pre-surgical circumferential strain in the A1 segment may be a good independent predictor of post-surgical 6 month recurrence of IMR.

**TABLE 1.**

Parameter values used in the constitutive equations used to model the mechanical response of MV tissue.

$\mu_m$ (kPa)	$c_0$ (kPa)	$c_1$	$E_{ub}$
10.11	0.0485	24.26	0.371

Author Manuscript

Author Manuscript

Author Manuscript

Author Manuscript